https://doi.org/10.5194/essd-2023-209
Preprint. Discussion started: 7 June 2023

Earth System Science Data
Open Access Discussions

Hyperspectral reflectance of pristine, ocean weathered and biofouled plastics from dry to wet and submerged state

Robin V. F. de Vries [1], Shungudzemwoyo P. Garaba [1, 2], Sarah-Jeanne Royer [1, 3]

[1] The Ocean Cleanup, Batavierenstraat 15, 3014 JH Rotterdam, The Netherlands
[2] Institute for Chemistry and Biology of the Marine Environment, Carl von Ossietzky University of Oldenburg, Schleusenstraße 1, Wilhelmshaven 26382, Germany
[3] Hawaii‘i Pacific University, The Center for Marine Debris Research, Hawaii‘i, USA

Correspondence to: Robin de Vries (robin.devries@theoceancleanup.com)

Abstract

High-quality spectral reference libraries are important for algorithm development and identification of diagnostic optical features of target objects in environmental remote sensing applications. We present additional measurements conducted using hyperspectral sensor technologies in a laboratory and outdoor setting to further extend high-quality data as well as diversity in available open-access spectral reference libraries. These observations involved gathering hyperspectral single-pixel point and multi-pixel optical properties of a diverse set of plastic materials (e.g., ropes, nets, packaging, and personal protective equipment). Measurements of COVID-19 personal protective equipment were conducted to also further expand reference datasets that could be useful in monitoring mismanaged waste related to the pandemic. The sample set consisted of virgin polymers and ocean-weathered and artificially biofouled objects of varying apparent colors, shapes, forms, thicknesses, and opacity. A Spectral Evolution spectroradiometer was used to collect hyperspectral reflectance single pixel point information from 280 – 2500 nm. Imaging was also performed using a Specim IQ hyperspectral camera from 400 – 1000 nm. Sampling underwater was completed in intervals of 0.005 m to 0.215 m within a 0.005 - 0.715 m depth range. All optical measurements are available in open-access for the laboratory experiment through https://doi.org/10.4121/769cc482-b104-4927-a94b-b16f6618c3b3 (de Vries and Garaba, 2023) and outdoors campaign involving the biofouling samples via https://doi.org/10.4121/7c53b72a-be97-478b-9288-ff9c850de64b (de Vries et al., 2023).

1 Introduction

Aquatic plastic waste is a threat to the socioeconomics and health state of the blue planet (Barboza et al., 2018; Beaumont et al., 2019; UNEP, 2021). Therefore, it is essential to have an interdisciplinary strategy for understanding the challenges and complexities related to global pollution by plastic waste. Among key approaches of scientific evidence-based research, remote sensing has emerged as a potential tool that could support monitoring the sources and sinks of this aquatic plastic waste (Maximenko et al., 2019; Van Sebille et al., 2020; Martínez-Vicente et al., 2019). The potential application of remote sensing technologies is ongoing, and promising findings have been reported from laboratory or mesocosm (Goddijn-Murphy and

https://doi.org/10.5194/essd-2023-209
Preprint. Discussion started: 7 June 2023

Dufaur, 2018; Garaba et al., 2021), ship (de Vries et al., 2021), aircraft (Garaba et al., 2018), satellite-based studies (Park et al., 2021; Topouzelis et al., 2019), and sensitivity analyses that combine laboratory measurements incomplete radiative transfer computations to top of the atmosphere (Garaba and Harmel, 2022).

At present, optical-based remote sensing methodologies gather multi- or hyperspectral radiometric quantities to investigate and determine diagnostic reflectance characteristics of plastic waste. The unique optical features in the visible to longwave infrared spectrum are essential as they help develop algorithms for detecting or distinguishing plastics from other optically active components of the natural environment (Garaba et al., 2020; Tasseron et al., 2021a; Guffogg et al., 2021). Furthermore, collecting diverse measurements is important in further expanding open-access spectral reference libraries considering the variability of optically active materials in the natural environment. Such diverse and extensive spectral reference libraries composed of well-curated end-member information are invaluable. They can be used to match unknown spectra with known materials using statistical metrics that evaluate the similarity in signal shape of the observed samples. To this end, there are ongoing efforts to produce high-quality open-access spectral reference libraries and fill the scientific data gaps (**Table 1**).

In this study, we describe a dataset that further adds to what is open-access by (i) increasing the depth resolution, including ranges at which submerged plastics were investigated, (ii) assessing the optical characteristics of active or freshly biofouled plastic samples, (iii) investigating reflectance properties using artificial laboratory-based as well as natural light in outdoor settings, (iv) sampling a diverse set of materials ranging from pristine, ocean weathered to personal protective equipment and (v) using a synergy of advanced technologies from imaging to point measurement tasks. The metadata attached to the measurements obtained in our study is anticipated to be of additional value in radiative transfer simulations aimed at understanding how remote sensing efforts could be affected by biofouling and the submersion of polymers.

Table 1: Comparison of open-access spectral reference libraries containing plastic materials.

Study	Scenarios	Water Depth Intervals	Depth Range (m)	Quantified sample thickness	Biofouling	Wavelength Range (nm)	Polymer Types
This dataset	Dry and Wet Submersion Biofouling	21▲, 4•	0–0.70	yes	Active Mesocosm Wet	280 – 2500▲, 400 – 1000•	PS, HDPE, PP, PET-G, PVC, XPS, PA6-XT, Other, Unknown
(Leone et al., 2023)	Dry and Wet Submersion Water Clarity Biofouling	4▲	0 – 0.08	yes	Mesocosm	350 – 2500▲	PE, PP, PET, PETa, PETc, PS, PVC, HDPE, LDPE, XPS, PA6, TPe, Fluorocarbon

https://doi.org/10.5194/essd-2023-209
Preprint. Discussion started: 7 June 2023

(Knaeps et al., 2021)	Dry and Wet Submersion Water Clarity	7$^{\blacktriangle}$	0 – 0.32	no	Natural Dry	350 – 2500$^{\blacktriangle}$, 280 – 2500$^{\blacktriangle}$	PET, LDPE, PP, Polyester, Uknown
(Garaba et al., 2021)	Dry and Wet Pixel Coverage Geometry	1$^{\blacktriangle}$	–	no	Natural Dry	350 – 2500$^{\blacktriangle}$	LDPE, HDPE, PP, PS, Unknown
(Tasseron et al., 2021b)	Dry and Wet	1$^{\bullet}$	–	no	Natural Dry	400 – 1000$^{\bullet}$, 1000 – 1700$^{\bullet}$	LDPE, HDPE, PS, PP, PET, PO
(Garaba et al., 2020)	Dry	1$^{\blacktriangle}$	–	no	Natural Dry	6000 – 14000$^{\blacktriangle}$	PET, PS, Unspecified
(Garaba and Dierssen, 2020)	Pellets and microplastic	1$^{\blacktriangle}$	–	no	–	350 – 2500$^{\blacktriangle}$	PVC, PA6, PA6.6, LDPE, PET, PP, PS, FEP, ABS, Merlon, PMMA

$^{\bullet}$imaging and $^{\blacktriangle}$ point measurements. * indicates variation in sample thickness related to pristine samples. ABS: terpolymer lustran 752; FEP: fluorinated ethylene propylene teflon; LDPE: low-density polyethylene; HDPE: high-density polyethylene; PA6: polyamide 6; PA6.6: polyamide 66; PE: polyethylene; PET: polyethylene terephthalate; PETa: polyethylene terephthalate amorphous; PETc: polyethylene terephthalate crystalline; PET-G: polyethylene terephthalate glycol; PMMA: polymethyl methacrylate; PO: polyolefin; PP: polypropylene; PS: polystyrene; PVC: polyvinyl chloride; and TPe: Thermoplastic elastomers.

2 Methods and materials

2.1 Laboratory experiment

2.1.1 Samples

A set of pristine plastics was selected as standard reference samples (**Figure 1** and **Table 1**). The pristine samples included high-density polyethylene (HDPE), polypropylene (PP), polyvinylchloride (PVC), polyamide 6 (PA6), polyethylene terephthalate glycol (PET-G), and expanded polystyrene (XPS). The thickness of these pristine samples was 1 mm, 5 mm, and 10 mm for all materials. The polymer materials were chosen based on occurrence in rivers and oceans, e.g. (Lebreton et al., 2018; GESAMP, 2019). These pristine samples had a fixed length and width of 0.3 m by 0.3 m and were sourced from Steon Engineering Plastics in Rotterdam, The Netherlands. The XPS styrodur, by exception, was obtained from Van Beek Art Supplies in The Netherlands.

https://doi.org/10.5194/essd-2023-209
Preprint. Discussion started: 7 June 2023

Weathered fishing nets, blue, and white fragments harvested by The Ocean Cleanup System 001/B from the Great Pacific Garbage Patch (GPGP) in 2019 were included in the sample set for this study (**Figure 1** and **Table 1**). A multilayer packaging bag was also included as weathered household waste.

The amount of waste associated with the COVID-19 pandemic was also considered relevant because the number of single-use items that were likely mismanaged could end up in the natural environment (Benson et al., 2021). The common single-use personal protective equipment was considered to be blue surgical gloves, surgical masks, and rapid antigen tests (**Figure 1** and **Table 1**).

Table 2 Overview of pristine (1 – 6) and harvested/weathered (7 – 16) samples. All pristine materials were square plates measuring 0.3 m x 0.3 m. The other materials were irregular in shape but made large enough to ensure 100% pixel coverage for the spectroradiometer.

ID	Polymer	Condition/appearance	Thickness (mm)
01	HDPE	Pristine plastic	1, 5, 10
02	PP	Pristine plastic	1, 5, 10
03	PVC	Pristine plastic	1, 5, 10
04	PET-G	Pristine plastic	1, 5, 10
05	PA6-XT	Pristine plastic	1, 5, 10
06	PS (XPS Styrodur anthracite)	Pristine plastic	1, 5, 10
07	PP (oceanic)	White weathered, biofouled, top	*~ 3*
08	PP (oceanic)	White weathered, biofouled, bottom	*~ 3*
09	HDPE (oceanic)	Blue, weathered, biofouled	*~ 1 - 3*
10	HDPE (oceanic)	Green Net	*Mesh of 2 mm twines*
11	HDPE (oceanic)	White/Gray Rope	*~5*
12	Multilayer Packaging	Coffee bean package outside	*<1*
13	Multilayer packaging	Coffee bean package inside	*<1*
14	PS	Blue/green foam, used	*20*
15	HDPE fabric + LDPE coating	White construction sail	*< 1*
16	HDPE fabric + LDPE coating	Green construction sail	*< 1*
17	HDPE fabric + LDPE coating	Brown construction sail	*< 1*
18	Unknown	Medical: Rapid Antigen tests, Top	*~ 5*
19	Unknown	Medical: Rapid Antigen tests, Bottom	*~ 5*
20	Unknown	Medical: Gloves, New	*< 1*
21	Unknown	Medical: Gloves, Weathered	*< 1*
22	Unknown	Medical: Facemasks, New	*< 1*
23	Unknown	Medical: Facemasks, Weathered	*< 1*

https://doi.org/10.5194/essd-2023-209
Preprint. Discussion started: 7 June 2023

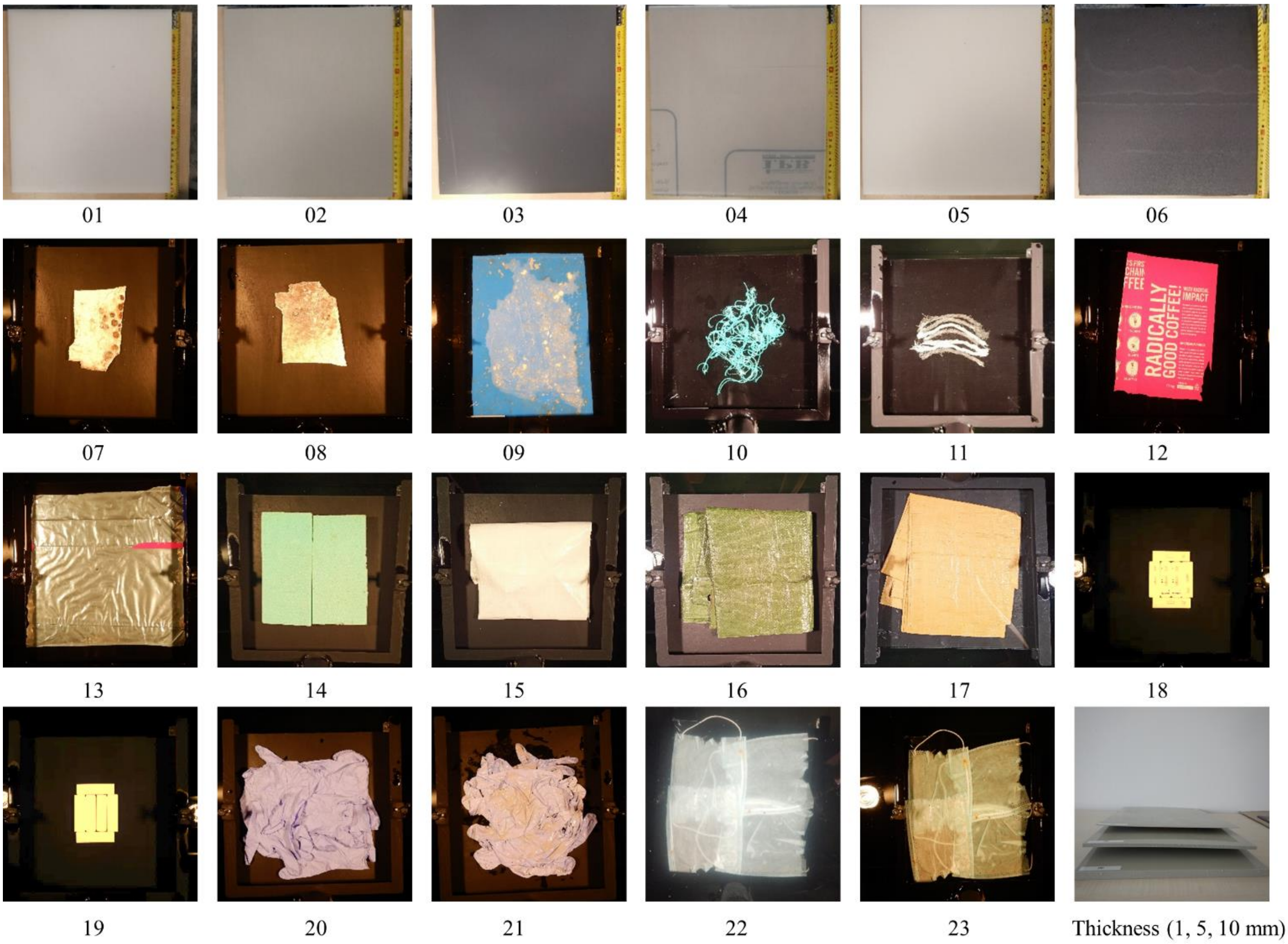

Figure 1 Overview photos of the sampled pristine (01 – 06) and weathered (07 - 23) plastics observed in August/September 2021 during the reflectance measurement campaign.

2.1.2 Experimental setup

Single pixel point measurements were completed using a hyperspectral Spectral Evolution SR-3501 (SEV) spectroradiometer from the Ultraviolet (UV, 280 nm) to Shortwave Infrared (SWIR, 2500 nm) with an 8° field-of-view lens attached. The sensor illuminates a circular swath, centered in the middle of the sample, with a growing diameter dependent on the sample submergence depth. The swath width is calculated using **Equation 1,** where *h* is the sensor-to-sample distance. Here the fixed sensor-to-water distance was 0.398 m. Optical refraction effects in the water-air interface were presumed negligible because all observations were made from the nadir at a 0° viewing angle and in calm water conditions. The maximum swath size was reached at the 0.715 m depth mark, where it reaches a diameter of 0.156 m.

https://doi.org/10.5194/essd-2023-209
Preprint. Discussion started: 7 June 2023

$$r_0 = h \cdot \tan\left(\frac{\alpha}{2}\right) \tag{1}$$

Relative reflectance was automatically determined at interpolated 1 nm spectral resolution by white referencing using a SphereOptics Zenith Polymer® SG3120 ≈ 99 % full material PTFE standard panel. Reference true colour images were obtained using a Nikon Coolpix W300 16 MP digital camera for each sample, except for the six homogeneous pristine plastic samples.

From a subset of irregular materials, we additionally collected hyperspectral imagery using a SPECIM IQ CMOS hyperspectral camera covering a wavelength range of 400 nm to 1000 nm with a spectral resolution of 7 nm. The camera has a 40 ° field-of-view with a 1.3 MP focus and a 5 MP viewfinder camera. SPECIM IQ imaging was done remotely using a USB connection to obtain real-time true colour images and initiate hyperspectral imaging via the SPECIM IQ Studio version 2019.05.29.2 software. White referencing to determine relative reflectance was completed using a standard white panel supplied by SPECIM IQ. Figure 2 shows the setup (a) and the samples (b) for which SPECIM hypercubes were collected, where the viewfinder image is shown adjacent to the RGB composite from the hypercubes.

2.1.3 Sample fixation and submergence

An aluminum pipe connected the sample holder to the main frame, allowing depth adjustments by unclamping, moving, and clamping the cylinder. The structure also provided movable mounting points for the spectroradiometer and imaging sensors. The frame itself could move along two rails on top of the tank. MOTIP black primer was sprayed on the frame part to mitigate background or stray light. The target area was illuminated by two ARRI Arrilite 750 Plus 575 W HPL halogen tungsten lamps set at 1.80 m above the ground directed at ~45 ° off the nadir on both sides of the tank. A 0.3 m x 0.3 m sample holder fixed the samples at progressive depths. To prevent sample buckling and consequent irregularities in the depth measurement, thin samples were further fixed by a glass window on top. All samples were supported by a 0.3 x 0.3 x 0.05 m black aluminum plate. The black aluminum plate was first abrased by 300-grain sandpaper, cleaned, degreased, and painted with a base layer of MOTIP EAN 8711347206407 black primer, then two layers of the blackest acrylic paint in the world, Black 3.0. The tank was filled with fresh water.

https://doi.org/10.5194/essd-2023-209
Preprint. Discussion started: 7 June 2023

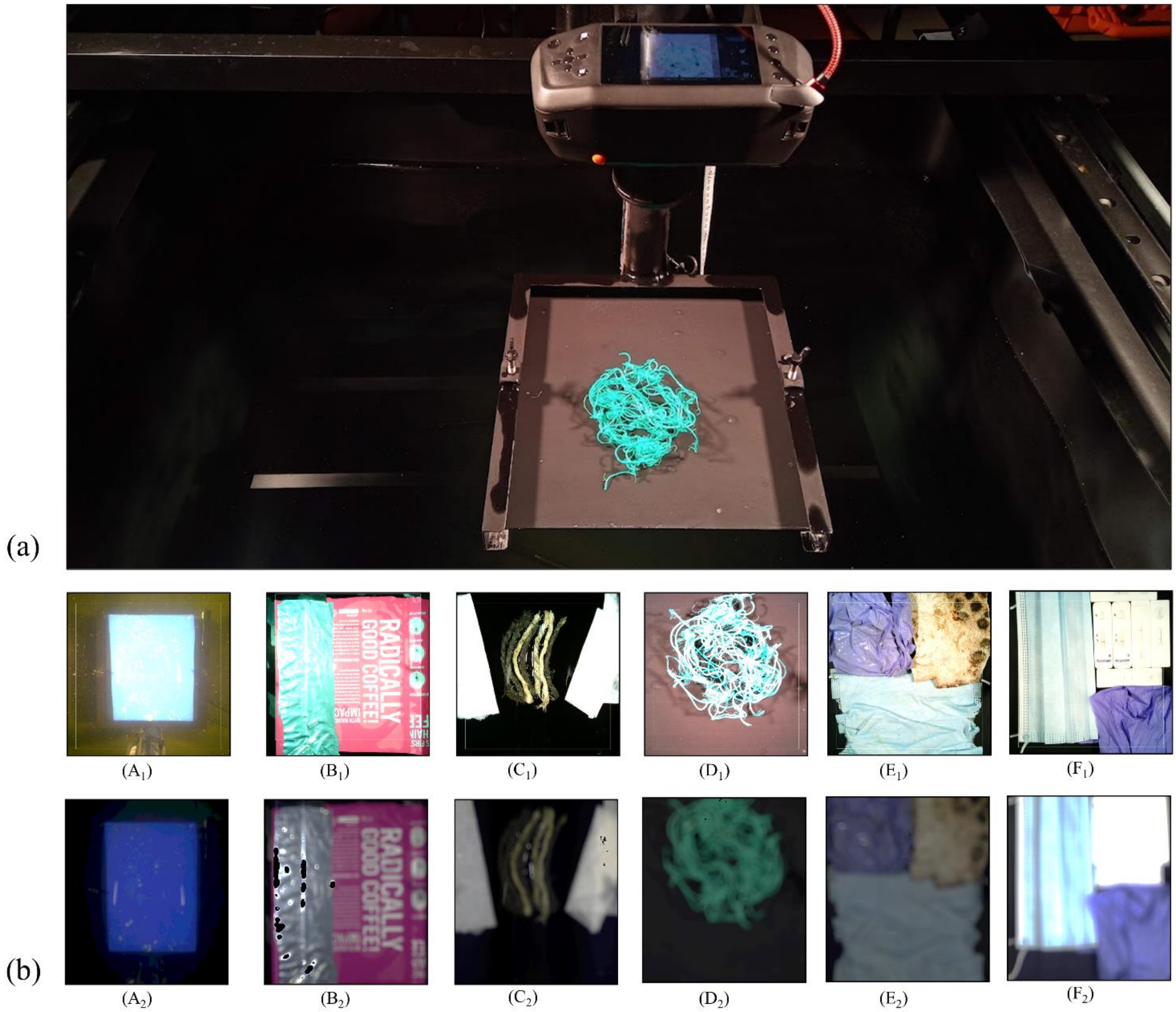

120 **Figure 2** (a) The SPECIM IQ camera, positioned over one of the samples, and (b) the samples that were recorded by the SPECIM IQ. Subscript (1) denotes the image taken from the viewfinder, and subscript (2) denotes the RGB composite from the SPECIM hypercube. The samples were: weathered ocean blue plastic front side (A), multilayer packaging, inside and outside combined (B), ocean rope (C), ocean green net (D), composite (old medical gloves, old medical face mask, white oceanhite plastic, (E)), and a composite of new face mask, new medical glove, and rapid antigen tests (F).

125 ### 2.1.4 Sampling procedures

Observations involved taking a measurement starting with the dry samples followed by intervals of submersion to depth, then finally just an above-water scenario of the wet target. The protocol was adopted from a prior study (Knaeps et al., 2021).

https://doi.org/10.5194/essd-2023-209
Preprint. Discussion started: 7 June 2023

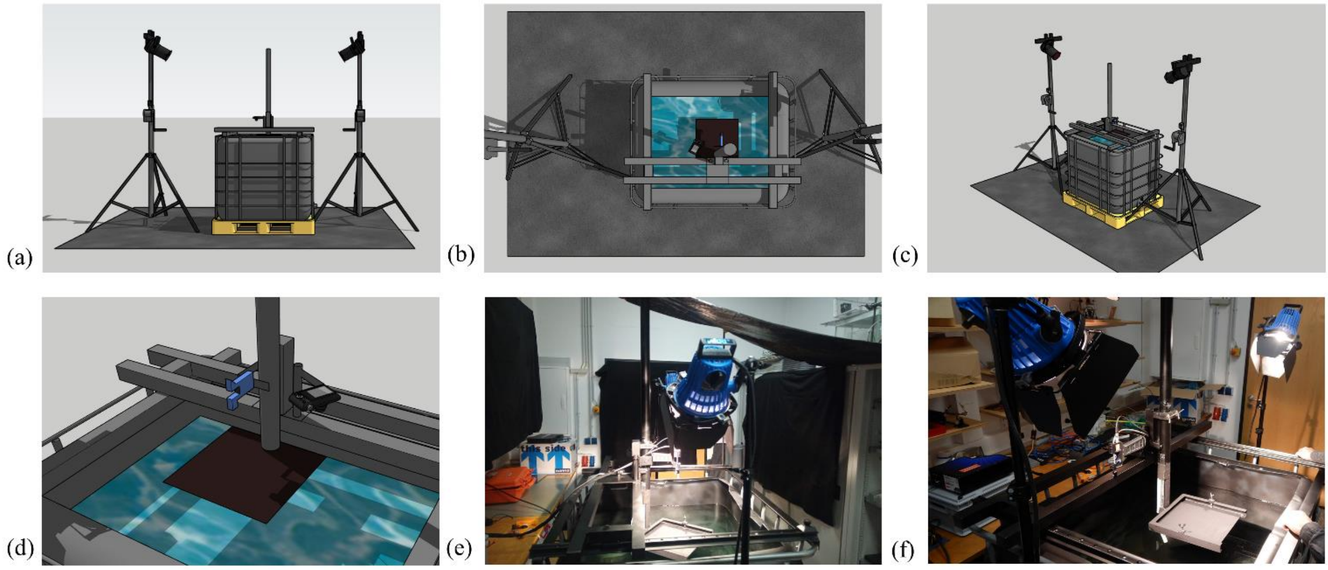

Figure 3 (a-d) Schematics and (c-d) true colour photos of the laboratory-based experimental setup with a dark container used to store the freshwater for submerged reflectance measurements. Background walls and frames were covered with dark fabric to mitigate stray light. Halogen tungsten lamps were used to provide artificial lighting above the tank at a ~45 ° nadir viewing angle.

2.1.5 Processing, data structures, and analyses of measurements

Raw data files from spectral measurements were converted into a PostgreSQL 14 database. The data structure was generated to combine all essential metadata (Figure 4). Custom scripts in Python 3.8.8 with Matplotlib 3.3.4 and Pandas 1.2.4 libraries were used to visualize the data. No additional processing was applied to the data.

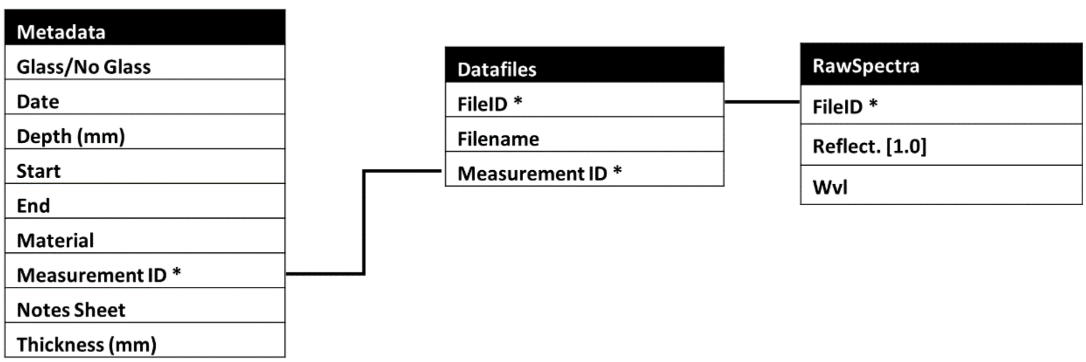

Figure 4 Data structure diagram for the hyperspectral measurement dataset. The table 'RawSpectra' contains the full set of raw data tables, concatenated from individual data files. The Metadata table contains the registration for each measurement and is linked to the RawSpectra through the Datafiles table. A Measurement ID from the Metadata table can have multiple FileIDS in the datafiles table. This also allows easy selection and aggregation of duplicate measurements for averaging and statistics.

https://doi.org/10.5194/essd-2023-209
Preprint. Discussion started: 7 June 2023

2.2 Outdoors mesocosm campaign

2.2.1 Samples and biofouling

Biofouling is ubiquitous in all-natural aquatic environments, but replicating it is a challenging task that requires a delicate balance of environmental parameters. To understand how biofouling influences the detectability of plastics from remote sensing optical technologies, we conducted a long-term mesocosm experiment within a flow-through aquaculture system on the sub-tropical island of Oʻahu in Hawaiʻi, USA. The samples were pristine panels of HDPE, PP, PVC, PA6, PET-G, and XPS, similar to polymers described before (**Section 2.1.1**). The panels were kept submerged in seawater to allow the biofilm to grow for 88 days from 15 June to 11 September 2022 (**Figure 5**). During the incubation time, environmental parameters such as pH, chlorophyll-a (Chl-*a*), salinity, nitrates, and phosphates were monitored weekly while light properties (UVA, UVB, PAR), dissolved oxygen, seawater temperature, and air temperature were recorded at higher temporal resolutions (days to minutes).

After the incubation period of 88 days, the samples were carefully transported from the flow-through aquaculture system in containers filled with seawater to the study site. Since the measurement campaign took place at a different location and due to the fragility of the biofilm and quick disintegration and decomposition when left out of the water, the samples were submerged in an adjacent seawater tidal canal to preserve the biofilm intact during the experiment. Each panel possessed a unique biofilm distributed on the surface of each panel (**Figure 5**).

https://doi.org/10.5194/essd-2023-209
Preprint. Discussion started: 7 June 2023

Open Access Earth System Science Data Discussions

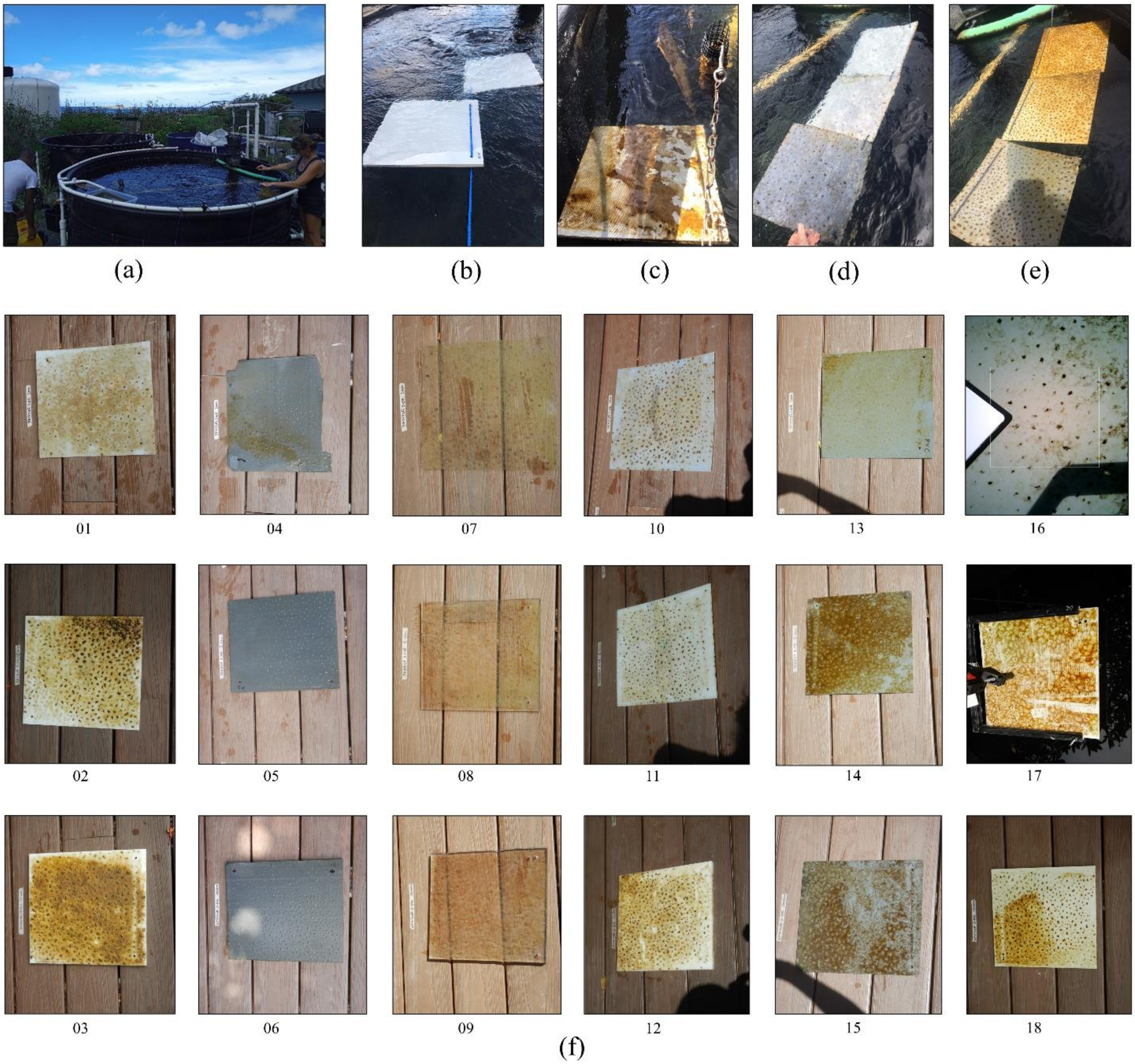

Figure 5 An overview of the biofouling tank (a); The sample biofouling process: (b) pristine samples are mounted in the tank, (c) the samples after a week of submersion, showing a biofilm which detached easily, (d) the bottom (tank-facing) of a sample set, after three months of biofouling, (e) the top (sky-facing) of the sample set, after three months of biofouling, and (f) overview of biofouled samples: HDPE (01 - 03), XPS (04-06), PET-G (07-09), PA6 (10-12), PVC (13-15), PP (16-18). Rows from top to bottom denote 1, 5, and 10 mm thickness, respectively. For PP 1 mm (16), the viewfinder preview of the SPECIM IQ camera is used as the overview image was found missing.

https://doi.org/10.5194/essd-2023-209
Preprint. Discussion started: 7 June 2023

2.2.2 Experimental setup

Hyperspectral point and multi-pixel measurements were conducted during daylight from 08:00 to 16:00 local time between 12 – 16 September 2022 on O‘ahu, Hawai‘i, USA (**Figure 6**). The outdoor measurements of the samples at 0, 5, 50, and 250 mm water depth were completed using the SEV spectroradiometer. However, the degree of buoyancy and fragility of the 1 mm thick XPS sample did not allow submersion, and hence measurements were only conducted at the surface. The panels were fixated by a U-shaped bracket (**Figure 6a**). Before collecting the spectral measurements, water layer depth was recorded with a ruler (**Figure 6a, b**). After the collection of all spectral reflectance measurements, the biofilm was carefully removed for further analysis (**Figure 6c**). The fore optic on the SEV was a 5° field-of-view lens and each measurement was an average of 20 scans (**Figure 6d**). The distance from the sensor to the water surface was 13 cm. The SPECIM IQ collected additional hypercube data of the biofouled samples at all water depths except above water (**Figure 6e**).

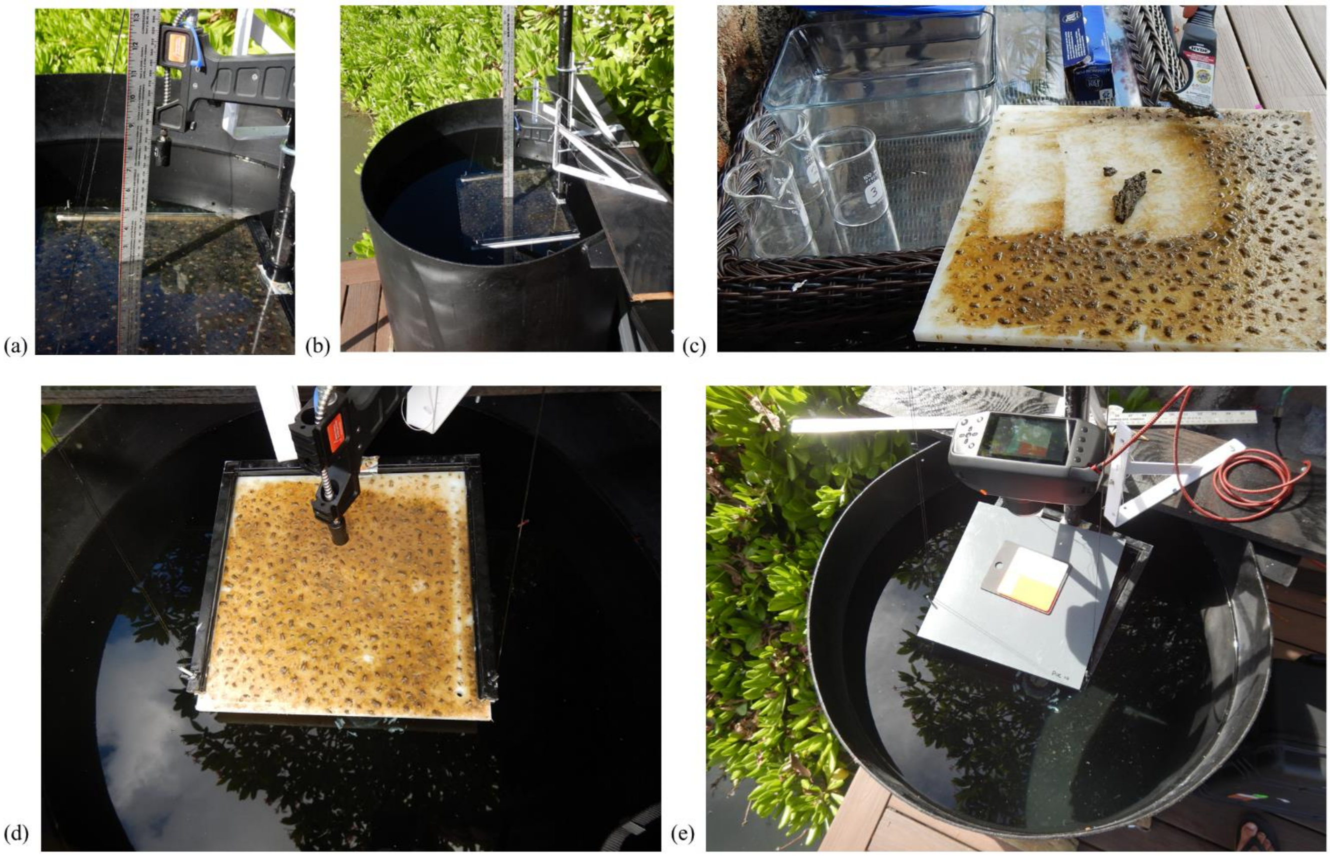

Figure 6 (a-b) Depth of submersion and distance of SEV lens to target measurements, (c) collection of biofilm to determine the biofilm mass for all the biofouled samples, (d) biofouled sample placed in position for SEV reflectance measurements and (e) SPECIM IQ camera collecting with a standard reference target.

2.2.3 Biofilm mass and thickness

A portable NiceGoodz electronic scale was used to determine the wet mass of the biofilm after removal from each panel (**Figure 6c**). Additionally, the thickness of the biofilm was estimated using a micrometer at three sample points. The pristine sample thickness was also recorded for reference against the manufacturer-reported thicknesses of the samples.

3 Results and discussion

3.1 SEV point measurements

3.1.1 Pristine samples

The spectral reflectance curves of the HDPE, PVC, PET-G, PA6, PP, and XPS panels with varying thicknesses and observed at depth are presented below (**Figure 7** and **Figure 8**), starting from a dry state just above the water surface (depth = 0 mm) and then followed by submerged observations. An increase in material thickness was revealed to cause an enhancement in the magnitude of detected reflectance for HDPE and PA6 but this was less pronounced in the other pristine plastics (**Figure 7** and **Figure 8**). It was also noted that for the thickest HDPE and PA6 samples, the inherent absorption features were enhanced in the near-surface water (0 – 50 mm) compared to thin samples. These PA6 and HDPE samples were semi-transparent which could influence these optical characteristics related to a direct correlation between thickness and signal magnitude. However, the fully transparent PET-G samples do not share the monotonic relationship between thickness and reflectance. Dark or transparent polymers tend to have a weak spectral reflectance even above water (e.g., XPS), which becomes weaker when submerged. Generally, the diagnostic absorption features appeared weak or relatively small in the SWIR for most thin plastics. This may have an impact on detectability in a noisy environment with other bright objects (i.e., with intense surface reflected glint, sea foam, breaking waves) or when the plastic pixel coverage is low.

We observed that the strong absorption of water in SWIR significantly affected the magnitude of reflectance measured for the pristine sampled with rapid loss of signal in the top layer (0 – 50 mm). From a first glance across all different polymer types, the SWIR (>1000 nm) part of the signal disappears beyond 50 mm water depth, while the visible domain (400 – 700 nm) remained present until the maximum depth of 70 cm. Even at 5 mm water depth, the spectral reflectance shape changes noticeably from the dry measurement for all polymer types investigated.

https://doi.org/10.5194/essd-2023-209
Preprint. Discussion started: 7 June 2023

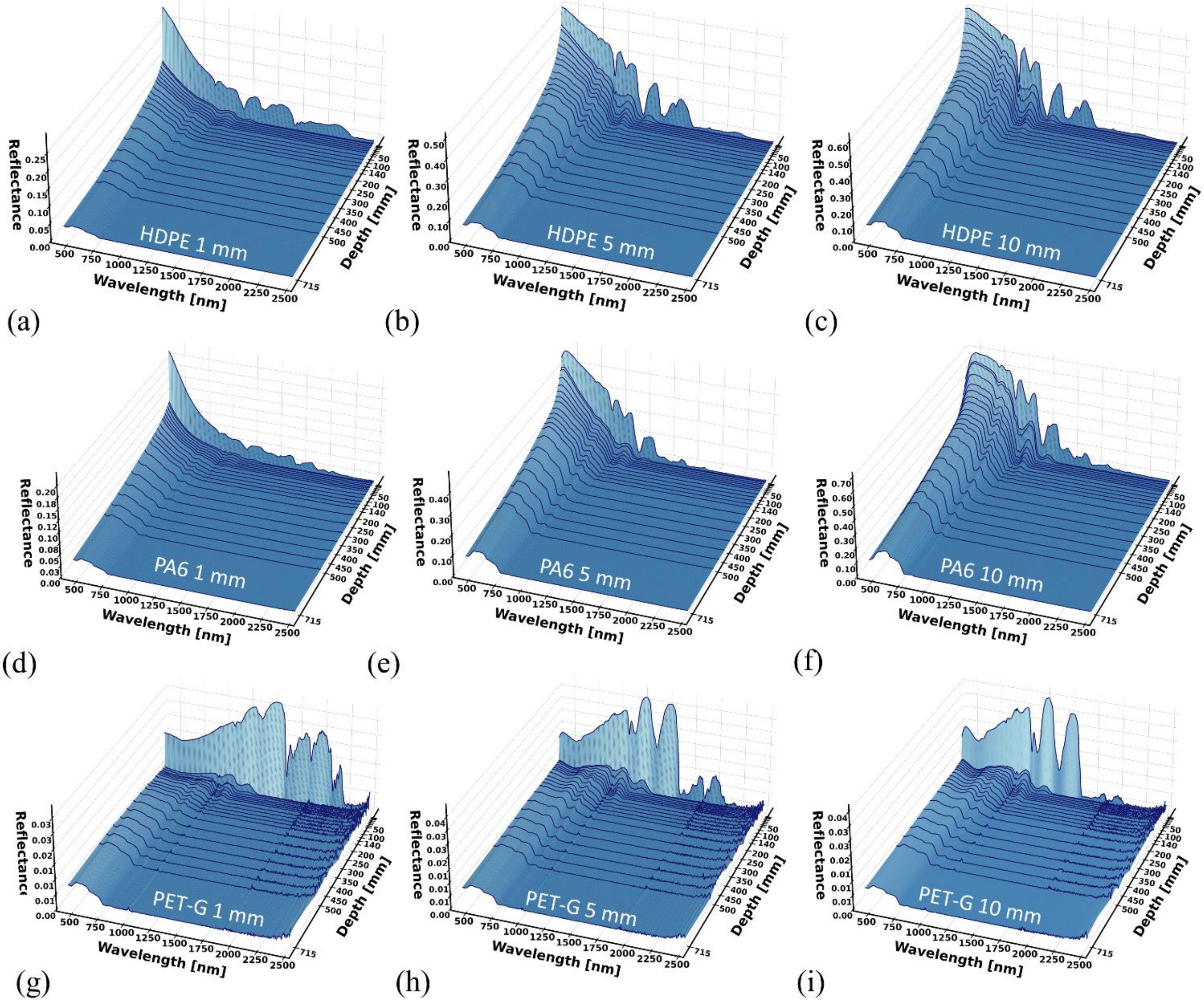

Figure 7 Spectral reflectance at varying depths for (a-c) HDPE, (d-f) PA6, and (g-i) PET-G for panel thickness ranging between 1 to 10 mm.

https://doi.org/10.5194/essd-2023-209
Preprint. Discussion started: 7 June 2023

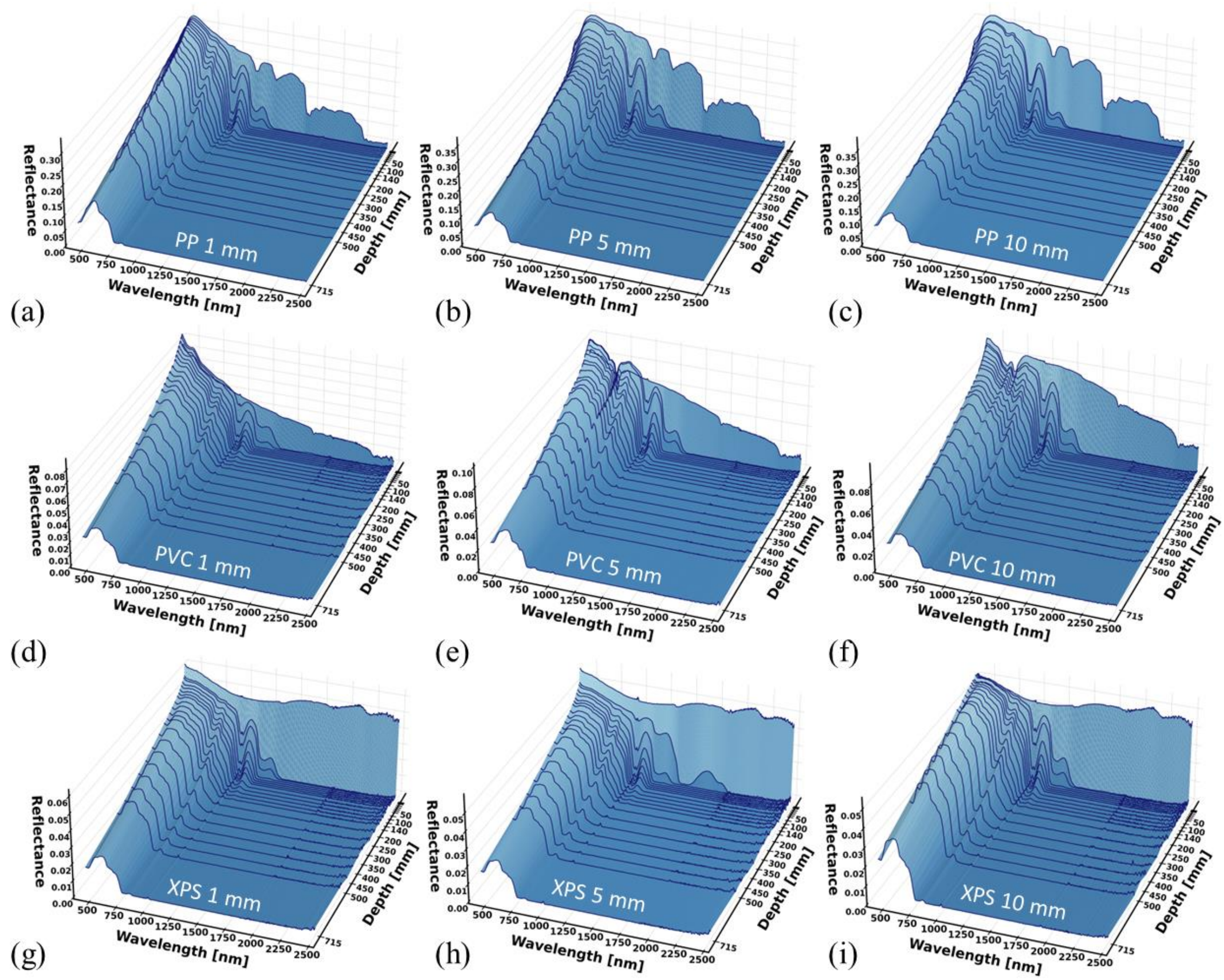

Figure 8 Spectral reflectance at varying depths for (a-c) PP, (d-f) PVC and (g-i) XPS for panel thickness ranging between 1 to 10 mm.

3.1.2 Construction materials, multilayer, and ocean-harvested, weathered plastics

Weathered materials were also measured and these included multilayer packaging (both sides), blue weathered ocean plastic, white weathered ocean plastic, green ocean net, and weathered ocean rope (**Figure 9**). A special case appears in **Figure 9a** (inside of the multilayer sample): around 500 nm, the reflectance increases with depth, mostly between 200 and 500 mm depth. This effect could be caused by variation of the lighting geometry with depth, combined with specular light reflection on the sample aluminum coating.

https://doi.org/10.5194/essd-2023-209
Preprint. Discussion started: 7 June 2023

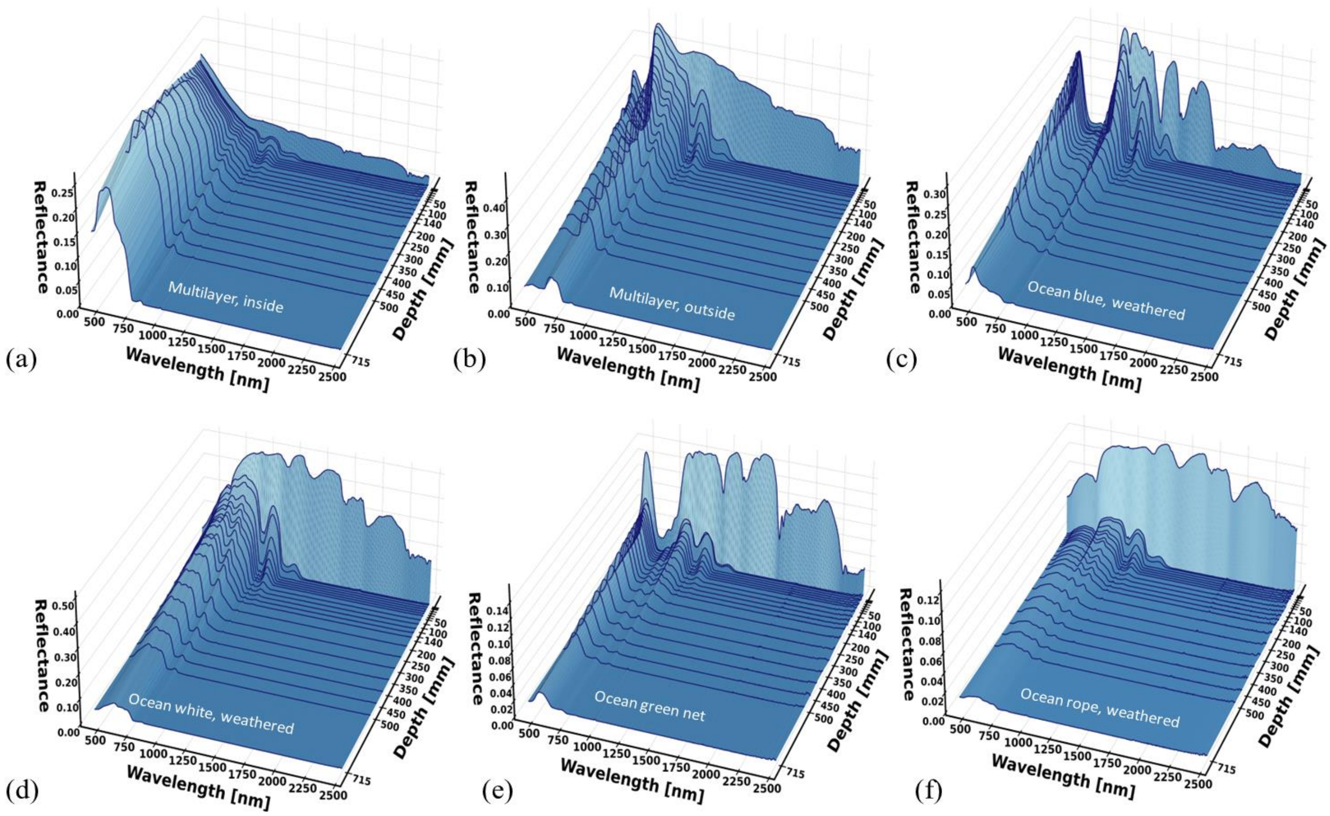

Figure 9 Spectral reflectance at varying depths for (a-b) multilayer inside and outside, (c) blue weathered ocean plastic,(d) white weathered biofouled dried ocean plastic, (e) a piece of green ocean net, and (f) weathered piece of ocean rope.

Blue foam, white, brown, and green sail pieces (items 14 – 17 in **Table 2**) spectral reflectance measurements were done at selected depths **(Figure 10)**. These weathered sailing pieces and a blue object were measured as representative items from nautical mismanaged waste. Peaks in the visible spectrum matched the apparent colours e.g., blue foam (~450 nm) and green sail (~550 nm). The blue foam had the highest reflectance in the SWIR whilst the lowest was found in the green sail.

https://doi.org/10.5194/essd-2023-209
Preprint. Discussion started: 7 June 2023

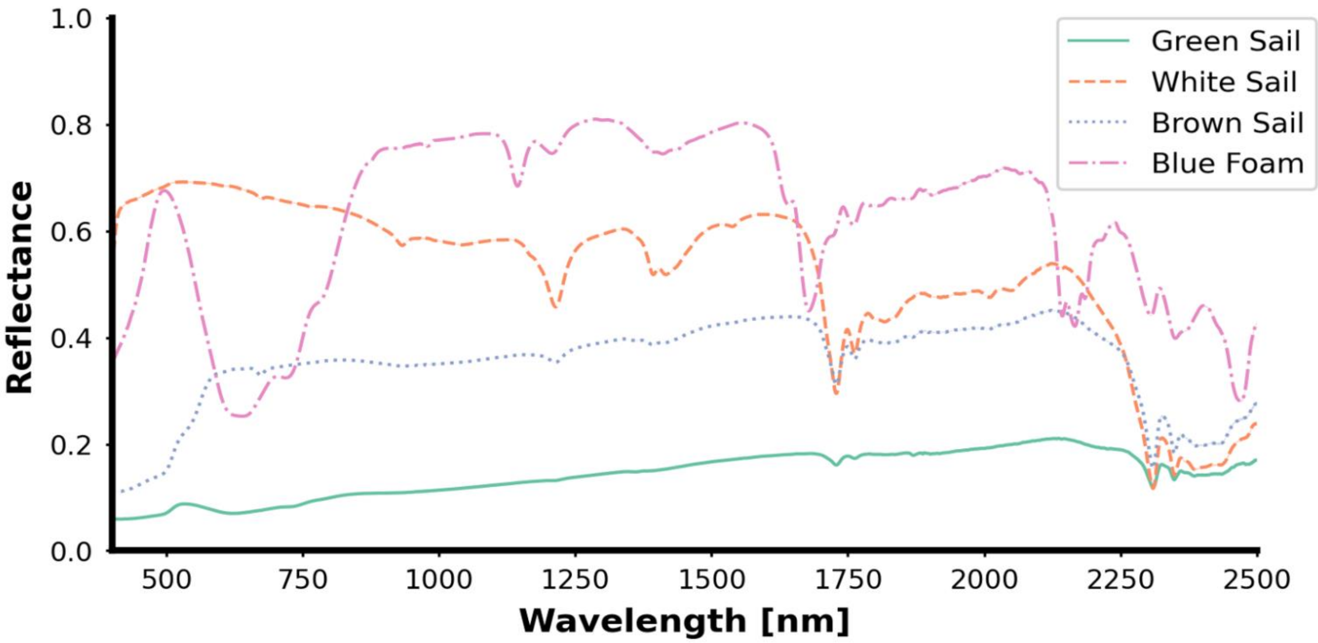

Figure 10 Spectral reflectance of sailing-related objects: white sail, sample ID 15 in Figure 1. (b): brown sail, sample ID 17 in Figure 1. (c): green sail, sample ID 16 in Figure 1. (d): blue foam, sample ID 14 in Figure 1.

3.1.3 COVID-19-related medical personal protective equipment (PPE)

Figure 11 presents an overview of the spectral reflectances for the different COVID-19-related PPE. Overall, the spectral reflectance values of (old) facemasks and gloves are visibly lower than those of the new samples. For medical gloves, both new and aged (**Figure 11a)** samples, above measurements were collected in a soaked and dry state. An aged, soaked medical glove has overall lower reflectance values. Above-water measurements of the facemasks (**Figure 11b**) were collected for both dry and soaked states. For the masks, soaking has a noticeable effect on the spectral reflectance. This effect becomes stronger when combined with the aging of the samples. Soaking of the old facemask even before submersion almost completely negates spectral reflectance values in most of the SWIR bands. Most of the remaining SWIR spectral reflectance is brought close to zero at 50 mm submersion depth. Finally, the measurements of RAT tests (**Figure 11c**) that were only taken above the water surface, reveal a small difference in reflectance for the top and bottom faces. The RAT test spectral reflectance curves show absorption features around 1150 nm, 1250 nm, and 1650 nm.

https://doi.org/10.5194/essd-2023-209
Preprint. Discussion started: 7 June 2023

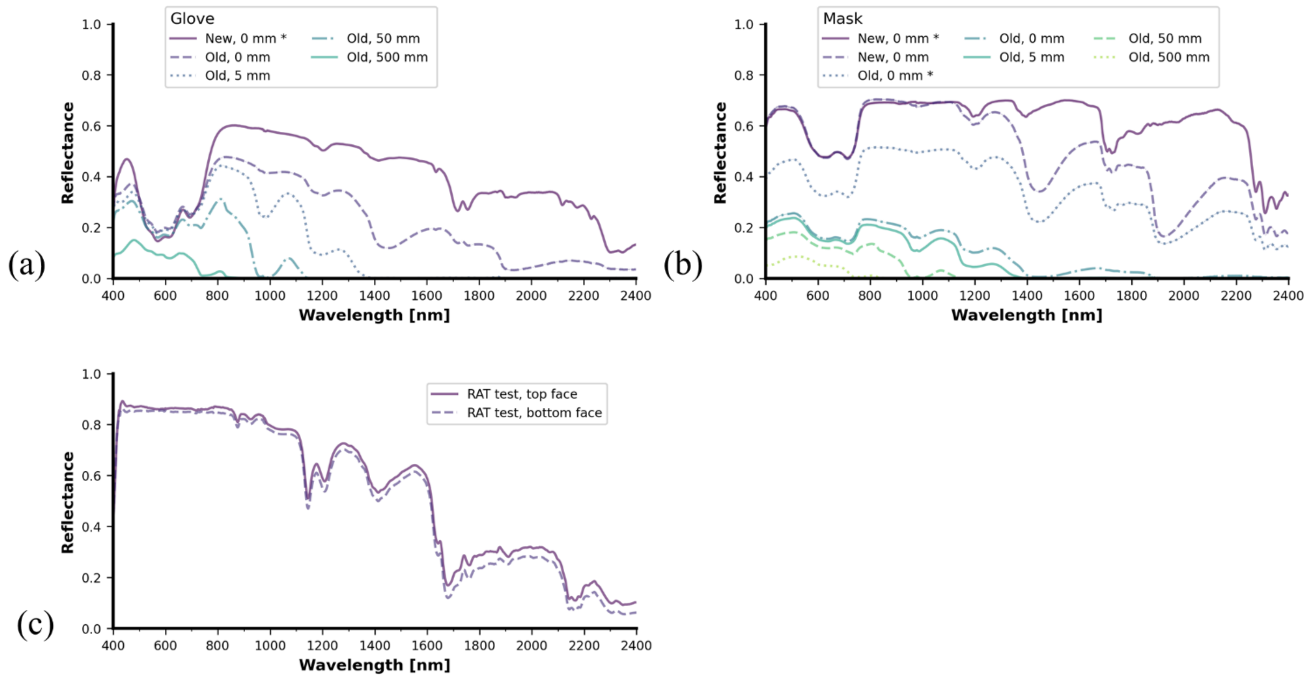

Figure 11 Spectral reflectance data from COVID-19-related medical waste in varying conditions: old and new medical masks from 0 to 500 mm depth (a), old and new surgical gloves from 0 to 500 mm depth (b), Rapid Antigen Tests (RAT, c). For medical masks and gloves, the * denotes that a sample was dry or fully drained after submersion.

3.1.4 Blank measurements

Blank measurements were obtained by taking reflectance measurements with no sample in the sample holder. (**Figure 12**) shows three types of blank measurements: with only water, the sample holder plate without a glass window, and the sample holder plate with a glass window. The water alone shows negligible reflectance over the observed spectrum. The presence of the sample holder was noted to have a reflectance contribution of at most 0.05 in the infrared. Over most of the spectrum, the

https://doi.org/10.5194/essd-2023-209
Preprint. Discussion started: 7 June 2023

reflectance values of the sample holder with the glass window are lower than the reflectance values of the sample holder without the glass window.

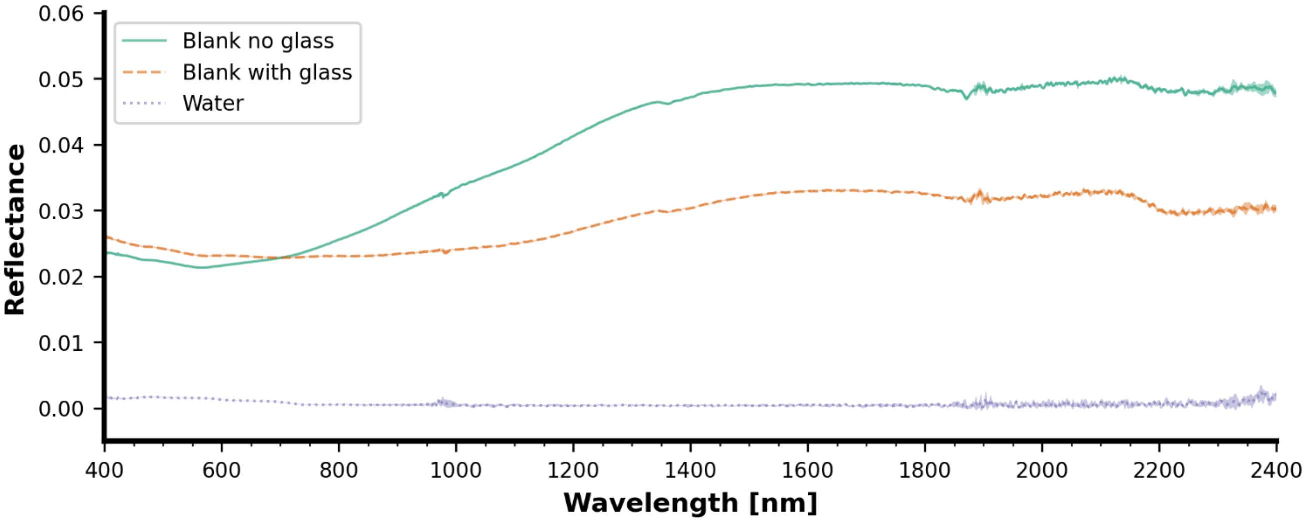

Figure 12 Comparison of different blank measurements above water. All sample measurements were taken with the 'Glass' or 'No glass' option, depending on the required setup. The black background plate has a higher reflectance than water. All measurements reported in this paper are raw measurements, meaning that the blank signal can still be subtracted to obtain material-specific reflectances with higher accuracy.

3.1.5 Biofouled samples

The wet mass and thickness of the biofilm on the pristine samples exhibit a direct positive relationship (**Table 3**). Biofilm thickness increased with sample thickness for HDPE, PP, and PA6. However, the variation of biofilm with substrate thickness seemed to be unclear for the other three polymers. The thickest and heaviest biofilm was found on the 10 mm HDPE samples.

Figure 13 compares the spectral reflectance of biofouled versus pristine samples for all the samples of 10 mm thickness. The spectral reflectance shape in the SWIR (> 1000 nm) domain remains largely unchanged. In contrast, most of the impact occurs in the visible spectrum (400 – 700 nm). Although the biofilm thickness varied among the different samples, this effect occurs for all samples, being most pronounced for HDPE (**Figure 13a)**, PS (**Figure 13b),** and PA6 (**Figure 13f)**. PET-G (**Figure 13c**) provides an exception in this case, as the biofouled sample was more reflective across the whole spectrum. Biofouled PP (**Figure 13d**) and PVC (**Figure 13e**) also both show a higher SWIR reflectance compared to the pristine samples. By comparing with the 50 mm depth measurement, it becomes clear that water depth plays the strongest part in reflectance attenuation above 1000 nm. None of the samples had extremely thick biofouling. Biofilms in the GPGP are expected to be even less significant in thickness and mass due to the oligotrophic marine environment in the open ocean. Yet, the biofilm grown on the samples in this study was relatively thick and representative of high-nutrient environments.

https://doi.org/10.5194/essd-2023-209
Preprint. Discussion started: 7 June 2023

275 **Table 3** Biofilm layer thicknesses and wet mass pristine plastic samples investigated between 12 – 16 September 2022 in Honolulu, Hawaiʻi, USA.

Polymer type	**Polymer thickness (mm)**	**Mean pristine thickness (mm)**	**Biofilm thickness (mm)**	**Mean wet biofilm mass (g)**
HDPE	10	9.84	2.24	22.60
	5	5.11	0.97	17.40
	1	1.20	0.09	4.27
PP	10	10.08	0.47	9.60
	5	5.09	0.35	2.43
	1	1.06	0.16	0.40
PS	10	9.91	0.73	2.00
	5	5.07	0.25	0.97
	1	0.83	0.12	1.17
PET-G	10	9.97	1.19	2.50
	5	4.86	0.25	1.40
	1	1.02	0.20	2.77
PVC	10	10.00	0.11	4.03
	5	4.88	0.20	3.93
	1	1.09	0.31	4.03
PA6	10	11.45	0.96	7.10
	5	5.25	0.77	3.80
	1	1.00	0.29	5.00

https://doi.org/10.5194/essd-2023-209
Preprint. Discussion started: 7 June 2023

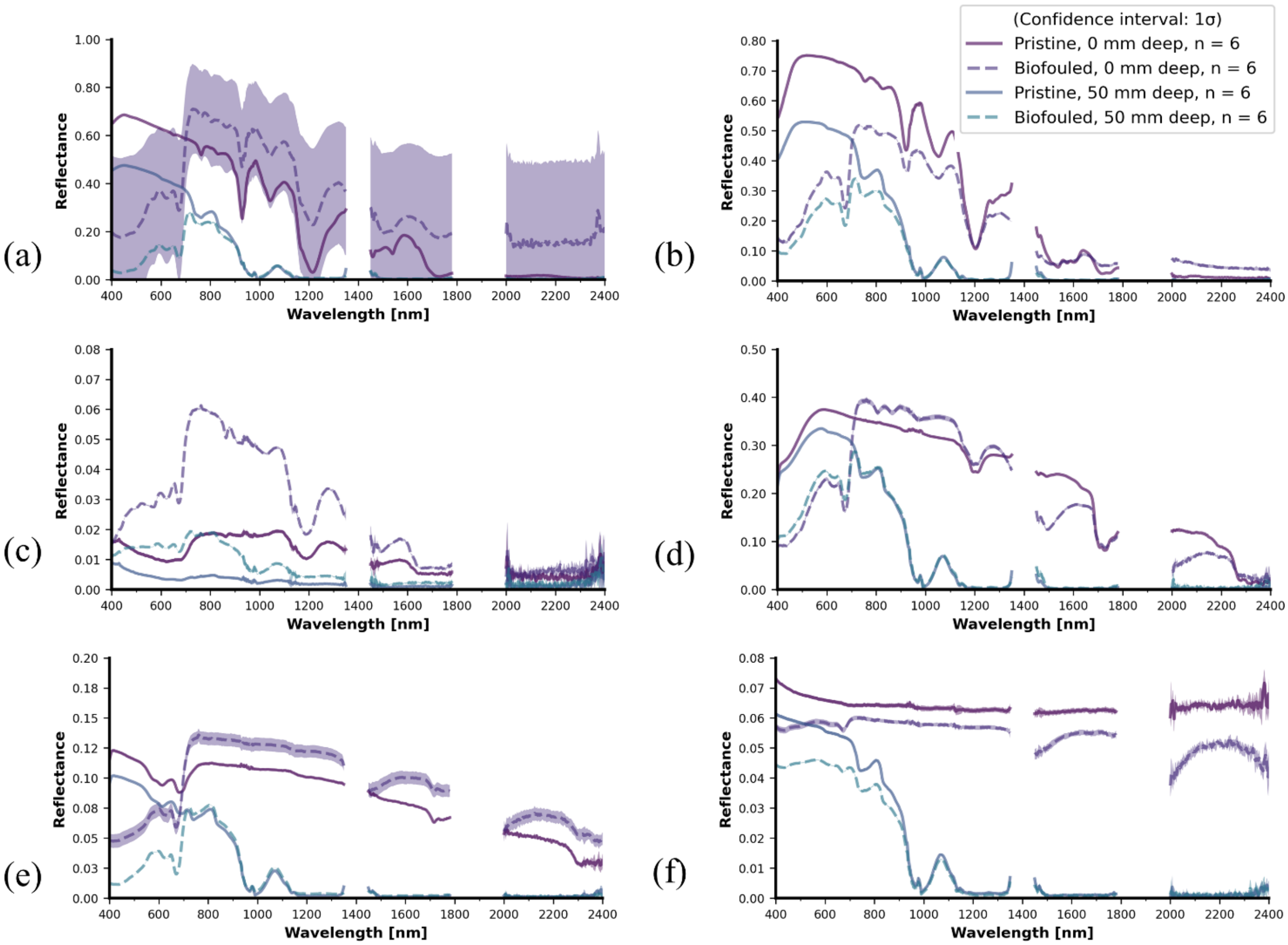

Figure 13 (a) 10 mm thickness HDPE, pristine and biofouled. The main difference occurs in the visible spectrum (400 – 700 nm), which is relatively dark. The biofilm does not obscure any of the typical spectral features; **(b)** 10 mm thickness PA6, pristine and biofouled. Here, the biofilm generally decreases the spectral reflectance magnitude, with the strongest diminishing effect in the visible (400 – 700) spectrum. Nevertheless, the spectral reflectance shape beyond 700 nm changes minimally; **(c)** 10 mm thickness PET-G, pristine and biofouled. The reflectance magnitude increases considerably across the entire spectrum for the biofouled sample compared to the pristine sample; **(d)** 10 mm thickness PP, pristine and biofouled. The main difference occurs in the visible spectrum (400 – 700 nm), which is relatively dark. Spectral features are not influenced by the biofilm; **(e)** 10 mm thickness PVC, pristine and biofouled. The biofilm mostly decreases the spectral reflectance magnitude in the visible (400 – 700 nm) spectrum. The spectral reflectance shape beyond 700 nm changes minimally; **(f)** 10 mm thickness XPS, pristine and biofouled. Only minimal differences occur, mainly in the < 700 nm part of the spectrum.

3.2 Specim IQ hypercubes

Figure 14 presents an example of several spectra obtained from the Specim IQ hypercube data: the dark background (A), a medical facemask (B), a medical glove (C), the marine-harvested and weathered white PP plastic (D), and the biofouled PP sample (E). The displayed reflectance curves are obtained by averaging ten points on each sample. Between the curves, we can distinguish the relatively high reflectance of the biofouled PP sample. Because the SPECIM IQ range is limited to 400 –

https://doi.org/10.5194/essd-2023-209
Preprint. Discussion started: 7 June 2023

1000 nm no information could be derived about the SWIR diagnostic features. Yet, the SPECIM IQ data is unique and offers the potential to further examine spatial heterogeneity of spectral reflectance on irregular samples. **Figure 14** also includes the standard deviation of each sample, obtained from different positions of the sample hypercube.

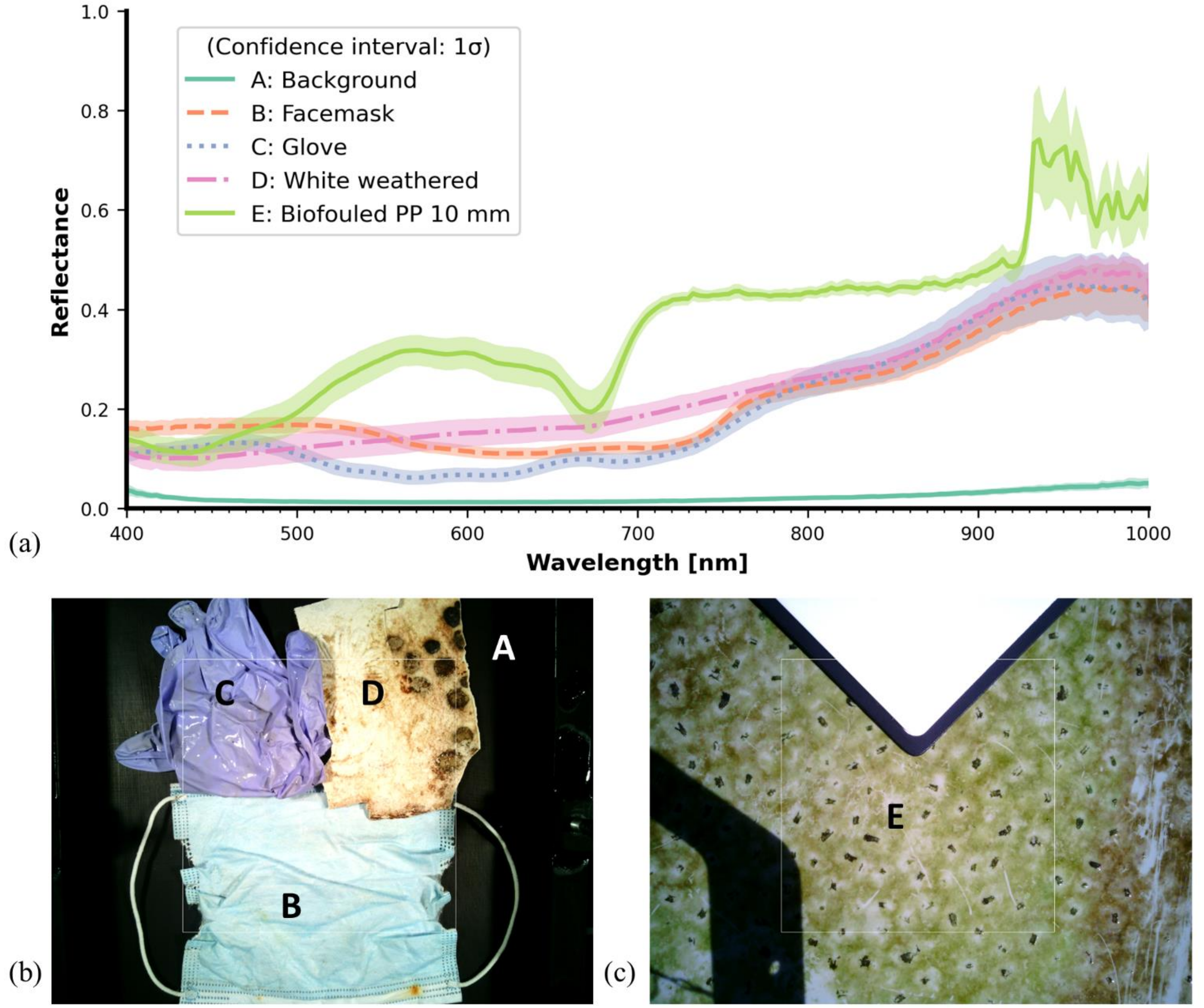

Figure 14 (a) Example spectra, aggregated from the SPECIM IQ hypercube data. For each of the spectral reflectance curves, at least ten points were sampled from the hypercube. The confidence intervals are obtained as the standard deviation of the data points across each sample. (b) The multi-material sample is represented by curves A, B, C, D. (c) Additional 10 mm thickness biofouled PP sample, represented by curve E.

https://doi.org/10.5194/essd-2023-209
Preprint. Discussion started: 7 June 2023

4 Data availability

The indoor laboratory data are available in open access through https://doi.org/10.4121/769cc482-b104-4927-a94b-b16f6618c3b3 (de Vries and Garaba, 2023). The outdoor experiment involving the biofouling samples is available at https://doi.org/10.4121/7c53b72a-be97-478b-9288-ff9c850de64b (de Vries et al., 2023).

5 Conclusions

This study presents and describes an open-access spectral reflectance dataset that was collected in an indoor and outdoor laboratory setting. This dataset provides an opportunity for the scientific community to further examine the relation between submersion in the water column, material properties, biofouling, and key diagnostic wavelengths for plastic marine litter.

Additionally, the data visualizations conducted here have already prompted several observations: Firstly, water depth has a strong influence on the spectral reflectance, as expected. Several diagnostic wavelengths in the SWIR spectrum become obscured at shallow (50 mm) water depths. Secondly, the material thickness influences the magnitude and contrast of spectral reflectance for several polymer types. The relation between material thickness and reflectance was strongest for HDPE and PA6. Finally, biofouling had a mixed effect on the spectral reflectance magnitude, depending on the material type and wavelength. However, the biofilm did not impact the shape of the spectral reflectance curve significantly in the SWIR. Water depth and material thickness appeared to remain the most significant factors for the spectral reflectance of floating and submerged plastic marine litter.

From a wider perspective and in comparison with recent comparable studies, the dataset presented in this study brings additional detail and range to the domain of hyperspectral remote sensing of plastic marine litter, by including COVID-19-related samples, ocean-harvested samples from the GPGP, live microcosm measurements and imaging. Furthermore, the inclusion of standardized pristine plastic samples is expected to increase comparability with other studies that have used the same standardized sample set.

https://doi.org/10.5194/essd-2023-209
Preprint. Discussion started: 7 June 2023

Open Access Earth System Science Data Discussions

Appendix A

325 **Figure A** displays the time series data of the environmental variables during the biofouling microcosm: air temperature, UV irradiance, PAR density, and seawater temperature.

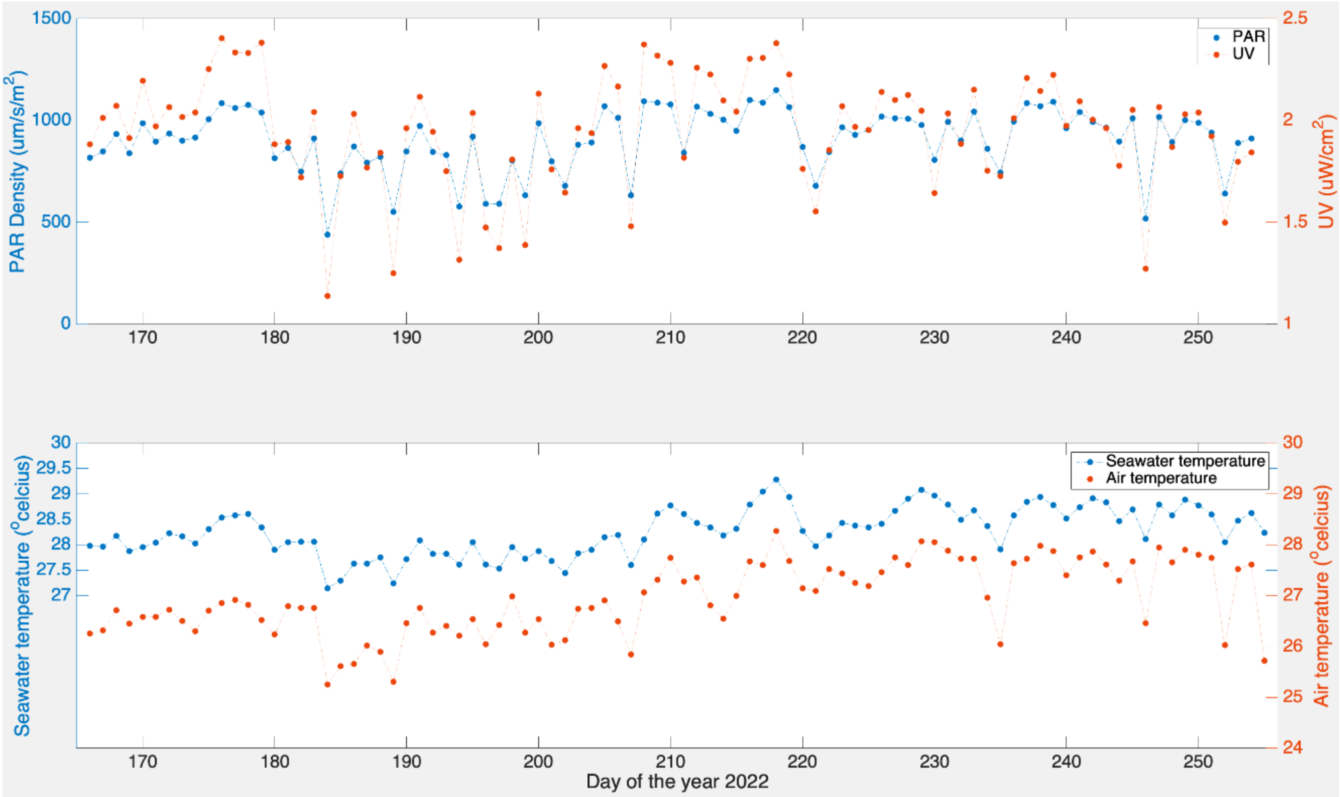

Figure A1: Daily average of the ultraviolet radiation (UV), photosynthetically active radiation (PAR), seawater, and air temperature measurements (°C) of the microcosm experiment from 15 June to 11 September 2022 during local daytime from
330 sunrise to sunset.

https://doi.org/10.5194/essd-2023-209
Preprint. Discussion started: 7 June 2023

Open Access Earth System Science Data Discussions

Appendix B

Table B1: Detailed characteristics of the biofilm on the biofouling microcosm experiment.

Polymer type	*Polymer thickness (mm)*	*Thicknesses (no biofilm) (mm)*			*Mean thickness (mm)*	*Std thickness (mm)*	*Thicknesses (with biofilm) (mm)*			*Mean thickness (mm)*	*Std thickness (mm)*	*Biofilm thickness (mm)*	*Weight (wet biofilm) (g)*			*Mean weight (mm)*	*Std weight (mm)*	*Weight (wet biofilm) (g) FACE DOWN*
HDPE	10	9.81	9.61	10.1	9.84	0.25	12.19	12.26	11.80	12.08	0.25	2.24	22.5	22.7	22.6	22.60	0.10	1
	5	5.01	5.14	5.18	5.11	0.09	5.94	6.86	5.45	6.08	0.72	0.97	17.3	17.6	17.3	17.40	0.17	1.1
	1	1.3	1.28	1.03	1.20	0.15	1.36	1.32	1.21	1.30	0.08	0.09	4.2	4.6	4	4.27	0.31	1
PP	10	10.05	10.23	9.96	10.08	0.14	10.40	10.77	10.49	10.55	0.19	0.47	9.6	9.5	9.7	9.60	0.10	1.5
	5	5.09	5.12	5.06	5.09	0.03	5.24	5.70	5.37	5.44	0.24	0.35	2.5	2.4	2.4	2.43	0.06	1.1
	1	1.06	1.06	1.07	1.06	0.01	1.16	1.19	1.32	1.22	0.09	0.16	0.4	0.5	0.3	0.40	0.10	0.1
PS	10	9.92	9.95	9.85	9.91	0.05	10.12	10.85	10.95	10.64	0.45	0.73	2.1	1.9	2	2.00	0.10	0
	5	5.02	5.09	5.1	5.07	0.04	5.16	5.48	5.33	5.32	0.16	0.25	1.1	0.8	1	0.97	0.15	0
	1	0.86	0.8	0.83	0.83	0.03	1.02	0.91	0.93	0.95	0.06	0.12	1	1.1	1.4	1.17	0.21	0
PET-G	10	10.01	9.96	9.94	9.97	0.04	11.11	11.58	10.79	11.16	0.40	1.19	2.5	2.4	2.6	2.50	0.10	2
	5	4.83	4.88	4.87	4.86	0.03	5.04	5.09	5.19	5.11	0.08	0.25	1.4	1.5	1.3	1.40	0.10	1.1
	1	1.02	1.03	1.01	1.02	0.01	1.17	1.20	1.30	1.22	0.07	0.20	2.8	2.8	2.7	2.77	0.06	0.8
PVC	10	9.98	10.01	10.02	10.00	0.02	10.14	10.09	10.10	10.11	0.03	0.11	4	4.1	4	4.03	0.06	3.2
	5	4.87	4.9	4.88	4.88	0.02	5.08	5.01	5.16	5.08	0.08	0.20	3.9	3.9	4	3.93	0.06	3.1
	1	1.1	1.07	1.1	1.09	0.02	1.42	1.46	1.33	1.40	0.07	0.31	4	4.1	4	4.03	0.06	1.1
PA6	10	11.52	11.41	11.43	11.45	0.06	12.48	12.44	12.32	12.41	0.08	0.96	7.1	7.2	7	7.10	0.10	2.8
	5	5.24	5.22	5.28	5.25	0.03	5.96	6.00	6.10	6.02	0.07	0.77	3.8	3.7	3.9	3.80	0.10	1.4
	1	1	1.01	1	1.00	0.01	1.24	1.31	1.34	1.30	0.05	0.29	5.1	4.9	5	5.00	0.10	1.5

https://doi.org/10.5194/essd-2023-209
Preprint. Discussion started: 7 June 2023

Open Access Earth System Science Data Discussions

Appendix C

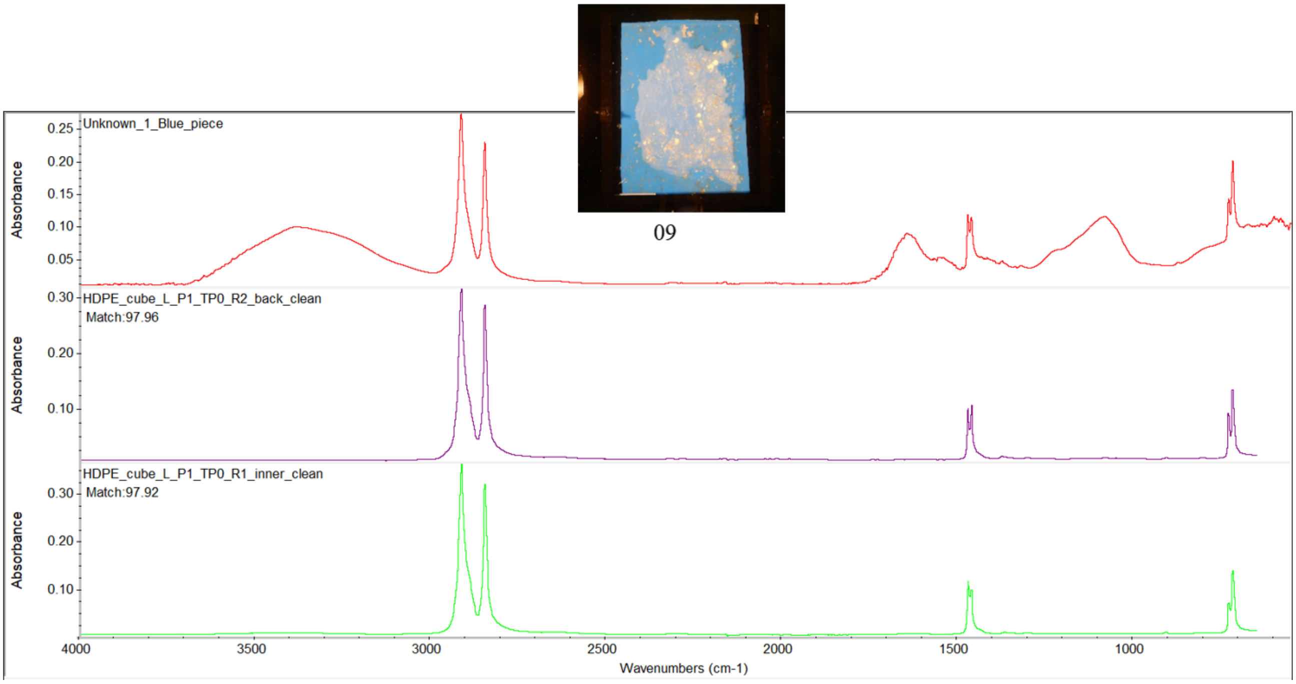

Figure C1: FTIR spectrum of the blue ocean-harvested plastic, indicating a match with HDPE.

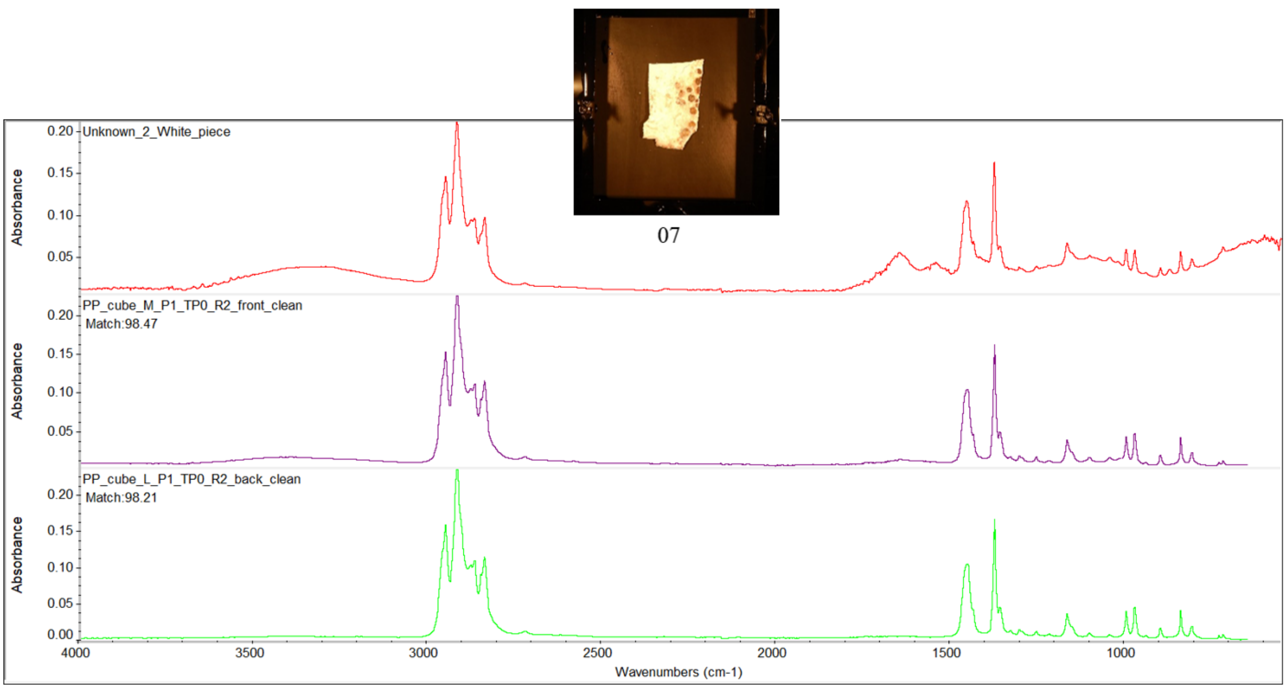

Figure C2: FTIR spectrum of the ocean-harvested white piece of plastic, indicating a match with PP.

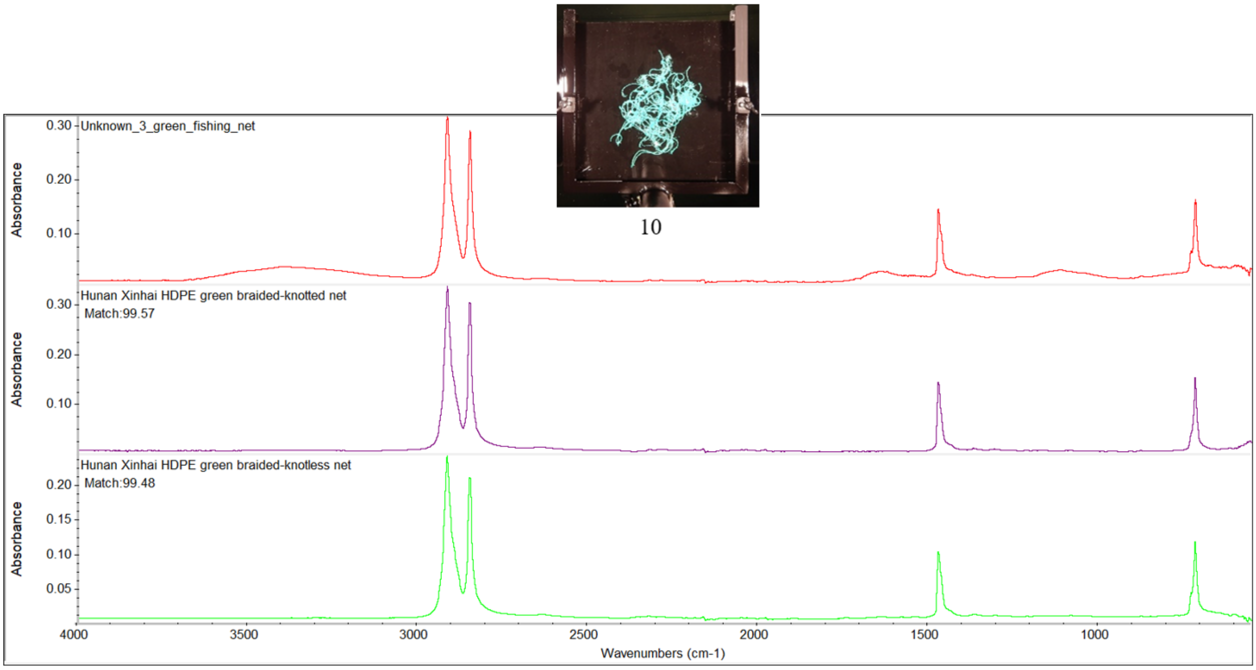

Figure C3: FTIR spectrum of the ocean-harvested green fishing net sample, indicating a match with HDPE.

Acknowledgments

We are grateful for the Wilhelmshaven tank construction by Gerrit Behrens, Helmo Nicolai, and Waldemar Siewert. We also thank Timo Sanders for the sample preparation, and Steon Engineering Plastics for supplying the pristine plastics. We thank the Hawai‘i Pacific University and the Center for Marine Debris Research for hosting the biofouling microcosm in their facilities. Finally, we thank Paolo Corradi of the European Space Agency for discussions about the study.

Author contribution

RdV, SPG, and S-JR designed the experimental setup and conducted the data collection and preparation. RdV performed project management, data quality control, data visualization, and preparation of the dataset for open access. All authors discussed and approved the manuscript text.

Competing interests

The authors declare that they have no conflict of interest.

Financial support

Funding for this work was from the Discovery Element of the European Space Agency's Basic Activities (ESA contract no. 4000132036/20/NL/GLC and 4000132037/20/NL/ GLC). SPG was also supported by the Deutsche Forschungsgemeinschaft grant no. 417276871.

References

Barboza, L. G. A., Dick Vethaak, A., Lavorante, B. R. B. O., Lundebye, A.-K., and Guilhermino, L.: Marine microplastic debris: An emerging issue for food security, food safety and human health, Mar. Pollut. Bull., 133, 336–348, https://doi.org/doi:10.1016/j.marpolbul.2018.05.047, 2018.

Beaumont, N. J., Aanesen, M., Austen, M. C., Börger, T., Clark, J. R., Cole, M., Hooper, T., Lindeque, P. K., Pascoe, C., and Wyles, K. J.: Global ecological, social and economic impacts of marine plastic, Mar. Pollut. Bull., 142, 189–195, https://doi.org/10.1016/j.marpolbul.2019.03.022, 2019.

Benson, N. U., Bassey, D. E., and Palanisami, T.: COVID pollution: impact of COVID-19 pandemic on global plastic waste footprint., Heliyon, 7, e06343, https://doi.org/10.1016/j.heliyon.2021.e06343, 2021.

Garaba, S. P. and Dierssen, H. M.: Hyperspectral ultraviolet to shortwave infrared characteristics of marine-harvested, washed-ashore and virgin plastics, Earth Syst. Sci. Data, 12, 77–86, https://doi.org/10.5194/essd-12-77-2020, 2020.

Garaba, S. P. and Harmel, T.: Top-of-atmosphere hyper and multispectral signatures of submerged plastic litter with changing water clarity and depth, Opt. Express, 30, 16553, https://doi.org/10.1364/oe.451415, 2022.

Garaba, S. P., Aitken, J., Slat, B., Dierssen, H. M., Lebreton, L., Zielinski, O., and Reisser, J.: Sensing Ocean Plastics with an Airborne Hyperspectral Shortwave Infrared Imager, Environ. Sci. Technol., https://doi.org/10.1021/acs.est.8b02855, 2018.

Garaba, S. P., Acuña-Ruz, T., and Mattar, C. B.: Hyperspectral longwave infrared reflectance spectra of naturally dried algae, anthropogenic plastics, sands and shells, Earth Syst. Sci. Data, 12, 2665–2678, https://doi.org/10.5194/essd-12-2665-2020, 2020.

Garaba, S. P., Arias, M., Corradi, P., Harmel, T., de Vries, R., and Lebreton, L.: Concentration, anisotropic and apparent colour effects on optical reflectance properties of virgin and ocean-harvested plastics, J. Hazard. Mater., 406, 124290, https://doi.org/10.1016/j.jhazmat.2020.124290, 2021.

GESAMP: Guidelines for the monitoring and assessment of plastic litter in the ocean, Rep. Stud. GESAMP, no 99, 130p, 2019.

Goddijn-Murphy, L. and Dufaur, J.: Proof of concept for a model of light reflectance of plastics floating on natural waters., Mar. Pollut. Bull., 135, 1145–1157, https://doi.org/10.1016/j.marpolbul.2018.08.044, 2018.

Guffogg, J. A., Blades, S. M., Soto-Berelov, M., Bellman, C. J., Skidmore, A. K., and Jones, S. D.: Quantifying marine plastic debris in a beach environment using spectral analysis, Remote Sens., 13, 1–23, https://doi.org/10.3390/rs13224548, 2021.

https://doi.org/10.5194/essd-2023-209
Preprint. Discussion started: 7 June 2023

Knaeps, E., Sterckx, S., Strackx, G., Mijnendonckx, J., Moshtaghi, M., Garaba, S. P., and Meire, D.: Hyperspectral-reflectance dataset of dry, wet and submerged marine litter, Earth Syst. Sci. Data, 13, 713–730, https://doi.org/10.5194/essd-13-713-2021, 2021.

Lebreton, L., Slat, B., Ferrari, F., Aitken, J., Marthouse, R., Hajbane, S., Sainte-Rose, B., Aitken, J., Marthouse, R., Hajbane, S., Cunsolo, S., Schwarz, A., Levivier, A., Noble, K., Debeljak, P., Maral, H., Schoeneich-Argent, R., Brambini, R., and Reisser, J.: Evidence that the Great Pacific Garbage Patch is rapidly accumulating plastic, Sci. Rep., 8, 1–15, https://doi.org/10.1038/s41598-018-22939-w, 2018.

Leone, G., Catarino, A. I., De Keukelaere, L., Bossaer, M., Knaeps, E., and Everaert, G.: Hyperspectral reflectance dataset of pristine, weathered, and biofouled plastics, Earth Syst. Sci. Data, 15, 745–752, https://doi.org/10.5194/essd-15-745-2023, 2023.

Martínez-Vicente, V., Clark, J. R., Corradi, P., Aliani, S., Arias, M., Bochow, M., Bonnery, G., Cole, M., Cózar, A., Donnelly, R., Echevarría, F., Galgani, F., Garaba, S. P., Goddijn-Murphy, L., Lebreton, L., Leslie, H. A., Lindeque, P. K., Maximenko, N., Martin-Lauzer, F.-R., Moller, D., Murphy, P., Palombi, L., Raimondi, V., Reisser, J., Romero, L., Simis, S. G. H., Sterckx, S., Thompson, R. C., Topouzelis, K. N., van Sebille, E., Veiga, J. M., and Vethaak, A. D.: Measuring marine plastic debris from space: Initial assessment of observation requirements, Remote Sens., 11, 2443, https://doi.org/doi:10.3390/rs11202443, 2019.

Maximenko, N., Corradi, P., Law, K. L., Sebille, E. Van, Garaba, S. P., Lampitt, R. S., Galgani, F., Martinez-Vicente, V., Goddijn-Murphy, L., Veiga, J. M., Thompson, R. C., Maes, C., Moller, D., Löscher, C. R., Addamo, A. M., Lamson, M. R., Centurioni, L. R., Posth, N. R., Lumpkin, R., Vinci, M., Martins, A. M., Pieper, C. D., Isobe, A., Hanke, G., Edwards, M., Chubarenko, I. P., Rodriguez, E., Aliani, S., Arias, M., Asner, G. P., Brosich, A., Carlton, J. T., Chao, Y., Cook, A.-M., Cundy, A. B., Galloway, T. S., Giorgetti, A., Goni, G. J., Guichoux, Y., Haram, L. E., Hardesty, B. D., Holdsworth, N., Lebreton, L., Leslie, H. A., Macadam-Somer, I., Mace, T., Manuel, M., Marsh, R., Martinez, E., Mayor, D. J., Moigne, M. Le, Jack, M. E. M., Mowlem, M. C., Obbard, R. W., Pabortsava, K., Robberson, B., Rotaru, A.-E., Ruiz, G. M., Spedicato, M. T., Thiel, M., Turra, A., and Wilcox, C.: Toward the Integrated Marine Debris Observing System, Front. Mar. Sci., 6, https://doi.org/10.3389/fmars.2019.00447, 2019.

Park, Y.-J., Garaba, S. P., and Sainte-Rose, B.: Detecting the Great Pacific Garbage Patch floating plastic litter using WorldView-3 satellite imagery, Opt. Express, 29, 35288, https://doi.org/10.1364/oe.440380, 2021.

Van Sebille, E., Aliani, S., Law, K. L., Maximenko, N., Alsina, J. M., Bagaev, A., Bergmann, M., Chapron, B., Chubarenko, I., Cózar, A., Delandmeter, P., Egger, M., Fox-Kemper, B., Garaba, S. P., Goddijn-Murphy, L., Hardesty, B. D., Hoffman, M. J., Isobe, A., Jongedijk, C. E., Kaandorp, M. L. A., Khatmullina, L., Koelmans, A. A., Kukulka, T., Laufkötter, C., Lebreton, L., Lobelle, D., Maes, C., Martinez-Vicente, V., Morales Maqueda, M. A., Poulain-Zarcos, M., Rodríguez, E., Ryan, P. G., Shanks, A. L., Shim, W. J., Suaria, G., Thiel, M., Van Den Bremer, T. S., and Wichmann, D.: The physical oceanography of the transport of floating marine debris, Environ. Res. Lett., 15, https://doi.org/10.1088/1748-9326/ab6d7d, 2020.

Tasseron, P., van Emmerik, T., Peller, J., Schreyers, L., and Biermann, L.: Advancing Floating Macroplastic Detection from

https://doi.org/10.5194/essd-2023-209
Preprint. Discussion started: 7 June 2023

Space Using Experimental Hyperspectral Imagery, Remote Sens., 13, 2335, https://doi.org/10.3390/rs13122335, 2021a.

Tasseron, P., van Emmerik, T., Schreyers, L., Biermann, L., and Peller, J.: Hyperspectral plastics dataset supplementary to the paper 'Advancing floating plastic detection from space using hyperspectral imagery,' https://doi.org/10.4121/14518278.v3, 2021b.

Topouzelis, K., Papakonstantinou, A., and Garaba, S. P.: Detection of floating plastics from satellite and unmanned aerial systems (Plastic Litter Project 2018), Int. J. Appl. Earth Obs. Geoinf., 79, 175–183, https://doi.org/10.1016/j.jag.2019.03.011, 2019.

United Nations Environment Programme: From pollution to solution: A global assessment of marine litter and plastic pollution, Nairobi, 148 pp., 2021.

de Vries, R., Egger, M., Mani, T., and Lebreton, L.: Quantifying Floating Plastic Debris At Sea Using Vessel-Based Optical Data and Artificial Intelligence, Int. Geosci. Remote Sens. Symp., 1118–1121, https://doi.org/10.1109/IGARSS47720.2021.9554154, 2021.

de Vries, R. V. F. and Garaba, S. P.: Dataset of spectral reflectances and hypercubes of submerged plastic litter, including COVID-19 medical waste, pristine plastics, and ocean-harvested plastics, https://doi.org/10.4121/769cc482-b104-4927-a94b-b16f6618c3b3.v1, 2023.

de Vries, R. V. F., Garaba, S. P., and Royer, S.-J.: Dataset of spectral reflectances and hypercubes of submerged biofouled, pristine, and ocean-harvested marine litter, https://doi.org/10.4121/7c53b72a-be97-478b-9288-ff9c850de64b.v1, 2023.